Scientific Research Publishing

Open Journal of Biophysics, 2024, 14, 339-354
https://www.scirp.org/journal/ojbiphy
ISSN Online: 2164-5396
ISSN Print: 2164-5388

Magnetic Field Emulations of Small Inhibitor RNA: Effects on Implanted GL261 Tumors in C57BL/6 Immune Competent Mice

Xavier A. Figueroa*, Gabriel Vogeli, B. Michael Butters

EMulate Therapeutics Inc., Bellevue, WA, USA
Email: *xfigueroa@emulatetx.com

How to cite this paper: Figueroa, X.A., Vogeli, G. and Michael Butters, B. (2024) Magnetic Field Emulations of Small Inhibitor RNA: Effects on Implanted GL261 Tumors in C57BL/6 Immune Competent Mice. *Open Journal of Biophysics*, **14**, 339-354.
https://doi.org/10.4236/ojbiphy.2024.144013

Received: July 13, 2024
Accepted: August 16, 2024
Published: August 19, 2024

Abstract

EMulate Therapeutics has developed a system for emulating the effects of solvated molecules via their magnetic field recordings. Recordings of magnetic field emissions of select small inhibitor RNAs (siRNAs; murine targeting CTLA-4 and murine targeting PD-1) were tested on C57Bl/6 mice implanted subcutaneously with the GL261 murine tumor cell line. A signal composed of concatenated recordings of siRNA molecules targeting the murine CTLA-4 and PD-1 receptors (labeled A2) was used in immune competent C57Bl/6 mice. The mice were flank implanted with the murine glioblastoma cell line GL261. Mice were exposed to the signal continuously (24 hours a day) until tumor volumes reached the designated volume limit. Tumors were excised and analyzed via PAGE/Western blot for the expression of CTLA-4, PD-1, Ki67, Caspase 3, CD4 and CD8. Terminal blood draws were used for CBCs. We report the down regulation of the checkpoint inhibitors CTLA-4 in the exposed mice. Significant tumor volume reduction was observed in mice exposed to the siRNA signal compared to control mice; no adverse events were recorded. Cell blood counts (CBC) and protein expression patterns were observed to correlate with the expected function of protein expression inhibition of the targets.

Keywords

Cytotoxic T-Lymphocyte Antigen 4 (CTLA-4), Programmed Cell Death Protein 1 (PD-1), Electromagnetic Field, Emulation, Cancer, Tumor, Murine, Glioblastoma Multiforme (GBM)

1. Introduction

EMulate Therapeutics (EMTx) has developed a technology that uses magnetic fields to emulate the electrostatic field of therapeutic molecules and their

therapeutic effects without ever administering the molecules to patients. Limitations imposed by physical drug pharmacokinetics/pharmacodynamics (PK/PD) are eliminated and delivery of our therapy (a time varying magnetic field) is dependent on the penetration of a magnetic field into tissue.

The theory used by EMTx, that surface charges are predominant and crucial for interaction in biological molecules and could be emulated via magnetic field recordings, is supported by published works in peer-reviewed literature. The publication of Thomas *et al.* [1] demonstrated that biological information could be transmitted with enough fidelity to induce molecule specific effects in neutrophils. The molecule 4-phorbol-12-β-myristate-13-acetate (PMA) is capable of inducing reactive oxygen species (ROS) generation in neutrophils [2], while 4-α-phorbol 12,13-didecanoate (PDD, an inactive PMA analogue) does not. Transmission of the PMA signal, via a magnetic field that was delivered to a neutrophil culture, resulted in the increase of ROS production by the neutrophils. The transmission of the magnetic field of a sample of the solvent or the inactive PDD did not produce measurable increase in ROS production.

The concept of measuring and recording an electrostatic field or electrostatic potential is derived from the recognition that the interaction between two molecules is through their molecular electrostatic potentials (MESP) [3]. The idea that one can derive structural information via the detection of the electrical potential of a molecule was recently demonstrated via escape-time electrometry [4]. Earlier work in protein modeling [5] demonstrated that it was sufficient to use the power spectrum of surfaces of the molecular electrostatic potential to successfully model proteins. This method was computationally less demanding, significantly faster than shape comparison methods and the power spectrum successfully assigned a unique fingerprint to each protein that was tested. The conceptual and theoretical framework of electrostatic surface potential (*i.e.* measuring the charge characteristics of a molecule) is slowly being developed. EMTx started from the theory that it was possible to record the magnetic field emanations of molecules via a pico- to tesla- scale magnetometer (MIDS SQUID) and a low-noise recording environment (the shielded MIDS system).

Demonstration that an electromagnetic signal emulates the mechanisms of action of the chemotherapeutic agents paclitaxel has been published, demonstrating the effect of the A1A signal [6]. The paclitaxel signal induces increased polymerization of α- and β-tubulin into stable microtubule bundles, producing effects similar to a physical paclitaxel molecule *in vitro* [6]. Additionally, independent corroboration of the effectiveness of the A1A signal has been published by the Kesari laboratory, in a flank U87 tumor model in mice [7]. U87, a human GBM derived tumor cell line, is inhibited by physical paclitaxel [8].

Human clinical trials in the United States and Australia have been conducted using the A1A signal (NCT02296580, NCT02507102) up to Phase II on recurrent glioblastoma (rGBM). The results demonstrate A1A safety and suggest equivalence to active therapies; additionally, synergies are detected when A1A and the best

standard of care are applied concurrently [9].

Other small molecules, like oligonucleotides, can be recorded using the EMTx technology and tested for therapeutic potential. EMTx technology has been able to target a specific gene product, epidermal growth factor receptor (EGFR), using the recording of a small inhibitor RNA (siRNA), to target human EGFR. The EGFR targeting siRNA signal effectively lowered EGFR mRNA levels, EGFR protein expression, reduced signaling pathway activity and increased survival time in animal models of glioblastoma and in patient derived tumor cell lines [10]. The Ulasov *et al.* [10] report demonstrates the ability of the EMTx technology to emulate small oligonucleotides.

The flexibility of siRNA technology and the proof-of-concept with EGFR siRNA signal allows us to develop therapeutic signals against established clinical targets. In the realm of cancer research and clinical treatment, two well-established targets in the immune checkpoint inhibition pathways are the cytotoxic T lymphocyte–associated protein 4 (CTLA-4) and programmed cell death protein 1 (PD-1) receptors. EMTx has recorded the magnetic field emissions of both siRNA targeting mouse and human CTLA-4 and PD-1. This signal, designated A2, can be delivered continuously in immune competent models and clinical cases. The A2 signal (mouse targeting siRNA sequences; https://www.emulatetx.com/s/Supplement-1-siRNA-constructs-V3.pdf) has shown activity against an *in vivo* mouse model implanted with the GBM GL261 cell line, as reported in [7].

Combined immunotherapies involving CTLA-4 and PD-1 have shown promise in non-small cell lung cancer [11] [12] and melanoma [13] [14] but the use of immunoglobulins carries the risk of side effects and adverse events triggered by the immune system [15]-[17]. Applying methods that eliminate immunoglobulin triggered adverse events, while targeting CTLA-4 and PD-1 receptor expression, would be an enhancement to a proven therapeutic target.

We hypothesized that we could detect a significant lowering of the CTLA-4 and PD-1 receptors using the siRNA targeting signal A2, partially replicating the proven benefits that have been shown in clinical trials that target CTLA-4 and PD-1 via immunoglobulins. The Mukthavaram *et al.* [7] published report demonstrated a clear effect in inhibiting tumor growth with the A2 signal. Additionally, a Phase I study, using the human version of A2, has demonstrated safety and a preliminary efficacy signal [18].

In this report, we present the results of digitally encoded signal mixtures (electromagnetic recordings of siRNA for CTLA-4 and PD-1) in reducing the tumor volume of implanted GL261 mouse-derived glioblastoma in immune-competent C57BL/6 mice. The A2 treatment led to a significant reduction in CTLA-4 expression compared to the control group and a shift in the CBC count for the lymphocyte population of exposed mice. Additionally, it supports the results of the Kesari laboratory [7], in which the A2 signal significantly reduced the tumor volume of implanted GL261 cells in immune competent C57Bl/6 mice.

2. Materials and Methods

2.1. Statistical Analysis

Tumor volumes were compared against controls using a one-tailed Student's T test, after an ANOVA. CBC counts and Western blot band densities were analyzed with a paired Student's T test, without correction for multiplicity of interactions.

2.2. Nucleotide Sequences

The CTLA-4 and PD-1 murine siRNA sequences were designed in-house (G. Vogeli) and produced by Dharmacon (GE, USA). A recording of the paclitaxel signal has been previously described [6]. All sequences were suspended in water from the manufacturer at a concentration of 40 μM and used to record the signal with the MIDS. Sequences are described in https://www.emulatetx.com/s/Supplement-1-siRNA-constructs-V3.pdf.

2.3. Sample Preparation

Samples preparation methods and results for the protein concentrations (via BCA protein assay) of each sample are listed in https://www.emulatetx.com/s/Supplement-2-PAGE-Western-Blots.pdf (Table 16, p. 16). Equal volumes of 10 mLs (40 mg) of sample were loaded per lane.

2.4. PAGE 1D Methods

SDS slab gel electrophoresis was carried out according to the method of Laemmli (Laemmli, U.K. Nature 227: 680-685, 1970) as described by Burgess-Cassler *et al.* (Clin. Chem. 35:2297-2304, 1989; second dimension) using a 10% or 5% acrylamide slab gels (125 mm length × 150 mm width × 0.75 mm thickness) overlaid with a 25 mm stacking gel. Electrophoresis was performed using 15 mA/gel for about 3.5 hrs. Each lance was loaded with After slab gel electrophoresis, the gels were placed in transfer buffer (10 mM CAPS, pH 11.0, 10% MeOH) and transblotted onto PVDF membrane overnight at 200 mA and approximately 100 volts/ two gels. The following proteins (Sigma Chemical Co., St. Louis, MO and EMD Millipore, Billerica, MA) were loaded in lanes as molecular weight standards: myosin (220,000), phosphorylase A (94,000), catalase (60,000), actin (43,000), carbonic anhydrase (29,000), and lysozyme (14,000). The PVDF membranes were stained with Coomassie blue R-250 and desktop scanned.

2.5. Western Blot Methods

Protein preparation and Western bots were done by Kendrick laboratories (Madison, WI). The Coomassie Brilliant Blue R-250 stained blots were desktop scanned, de-stained in 100% methanol, rinsed briefly in Tween-20 tris buffer saline (TTBS), and blocked for two hours in 5% nonfat dry milk (NFDM) in TTBS. Coomassie staining was done to assess the quality of the transfer and to ensure consistency between the gel transfers. The blots were then incubated in

primary antibodies diluted in 2% NFDM TTBS overnight and rinsed 3 × 10 minutes in TTBS. All the antibodies used in Western blots are listed in https://www.emulatetx.com/s/Supplement-2-PAGE-Western-Blots.pdf (Table 17, p. 16). Secondary antibody was a mouse anti-rabbit antibody conjugated to HRP and was purchased from GE Biotechnology. The blots were then placed in secondary antibody (anti-rabbit IgG-HRP [GE Healthcare Cat # NA 934V Lot # 9670531) diluted 1: 2000 in 2% NFDM TTBS for two hours, rinsed 4 × 10 in TTBS, treated with ECL, and exposed to x-ray film.

2.6. Band Quantification

The films were scanned with a laser densitometer (Model PDSI, Molecular Dynamics Inc, Sunnyvale, CA). The scanner was checked for linearity prior to scanning with a calibrated Neutral Density Filter Set (Melles Griot, Irvine, CA). Phoretix 1D v11.2 was used for lane selection, background subtraction, band selection and quantification of band volume. All band intensity values are normalized to the positive protein control for each Western blot.

2.7. Cell Culture Reagent, Cell Lines

A murine derived brain cancer tumor cell line (GL261) was a kind gift from the Kesari laboratory (Moores Cancer Center, UCSD). Cell propagation was done using standard *in vitro* cell expansion methods; in summary, cells were grown in DMEM (89%) + FBS (10%) + Penicillin and Streptomycin (1%). The cells were cultured in an incubator with 5% CO_2, 37.0˚C, and 80% humidity. Cells were harvested with Trypsin (0.05% Trypsin/0.53 mM EDTA in HBSS without sodium bicarbonate, calcium & magnesium). Cells were grown and sub-cultivated in T-175 flasks to confluence with every 2 - 3 day media renewals as appropriate until an adequate number of cells were obtained.

2.8. Mouse Strain, Tumor Implantation and Exposure Procedure

C57BL/6 female mice (6 - 8 weeks; 24 - 28 g) were purchased from Charles River (U.S.A., California). Mice were acclimated for 3 - 5 days prior to tumor implantation. GL261 cells (3×10^6 total cells/implant) were suspended in Matrigel (Corning, USA) 50 ul + PBS (50 ul) and the implanted tumor allowed to grow to ~75 mm^3. Mice were randomized into treatment and control cages prior to RFE exposure with the Voyager device. Control mice were kept in the same room as the treatment mice but not exposed to the A2 signal. All mouse studies were performed according to the standards set forth by IACUC at the Infectious Disease Research Institute (IDRI). All mice had access to rodent chow and water *ad libitum*. A12-hour light/12-hour dark photoperiod was maintained, except when room lights were turned on during the dark cycle to accommodate device change out. Room temperature was maintained between 24˚C - 26˚C. Animal room and cage cleaning was performed according to PSISOP. A transmission antenna was designed and used to expose mice to the Voyager signal. The signal had an average

field strength of ~40 mGauss. All mice were monitored daily for signs of distress, injury and survival. Mice were euthanized if tumors exceeded 2500 mm^3. Study was designed with a defined end-point of 25 days post-tumor implantation.

2.9. Signal Transmission and Coil Design

The Voyager device, a commercial grade RFE transmitter, was used to deliver the digitized signal to the antennas for the mouse experiments. The signal transmission system is described here [19]. The exposure apparatus is described previously [7]. Briefly, the mice (inside a plastic cage) are placed on a flat, rectangular coil that emits the digitally encoded signal as a radio (magnetic) emission. Whole body exposure occurs for all the mice in the antenna emission envelope. Briefly, the A2 signal was transmitted at levels of ~40 mGauss. The signal was set in a 6-minute cycle, transmitting signals in 3-minute blocks and cycling through a sequence of recorded signals. The signal then restarted and repeated the sequence.

2.10. Signal Acquisition and Selection

A custom-built electromagnetic isolation and recording chamber, Molecular Interrogation and Data System (MIDS), was designed to measure time sequences of non-stimulated magnetic field (MF) perturbations from molecules suspended in PBS and is described in a previous publication [6]. Briefly, MIDS is a specialized, low temperature (liquid Helium) superconducting quantum interference device (SQUID), inside a shielded chamber, housed inside a low temperature shielded Dewar; the gradiometer is connected to a data acquisition system. The low temperature SQUID coupled to a gradiometer detects small oscillations in the magnetic field over short time periods and converts these oscillations into voltage sequences. Signals of the nucleotide samples were recorded for 60-second intervals, digitized using proprietary software, and stored as a WAV file (Microsoft format).

Samples of siRNA, chemically modified, nucleic acids designed to specifically bind to and inhibit endogenous microRNA molecules were re-suspended in RNASE free PBS at a concentration of 40 μM and recording made of the electromagnetic emissions of the oligonucleotides.

Signals were selected from the MIDS, using a frequency analysis package in FlexPro8 (DEWETRON GmbH, Parkring 4, A-8074 Graz-Grambach, Germany). In short, the digitized data from FlexPro8 plots of the signals were converted from the time domain into the frequency domain using a Fast Fourier Transform algorithm and then analyzed by plotting the spectrum after autocorrelation. The signals were selected for high signal-to-noise, low interference and low entropy.

2.11. Cell Blood Counts (CBCs)

All CBCs were carried out by Phoenix laboratories (Seattle, WA). Mice were not fed or given water 8 hours before blood draws. Blood draws were terminal cardiac punctures and blood samples were blinded.

3. Results

3.1. Effects on Tumor Volumes and Complete Blood Counts in Whole Mouse Exposure to the RFE siRNA Signal A2 (-CTLA-4/-PD-1)

An independent study by the Kesari laboratory has previously described the effects of the A2 signal [7]. The same experimental set-up was used at the Infectious Disease Research Institute (IDRI), where the experimental exposures were done. Two separate runs were done to assess the growth rate of the GL261 tumor on C57Bl/6 mice, implanted in the right flank, with a total of 22 mice in the control group and 15 mice in the A2 WAV signal exposure group.

The average tumor volumes are displayed in Figure 1(a), demonstrating a reduced tumor growth rate in the A2 WAV signal group that is significant starting on Day 4 and continuing up to Day 25. By Day 25, the differences in tumor volumes between the two populations was P = 0.043 (a = 0.05).

In order to determine if the difference between the two populations was due to a subset of the largest tumors within the groups, three of the largest in the A2 WAV exposure group tumors and four of the largest tumors in the Control group were excluded from a second analysis (Best Responders). As displayed in Figure 1(b), the variability in both groups is reduced, but the difference between the two tumor populations remains significant (P = 0.039).

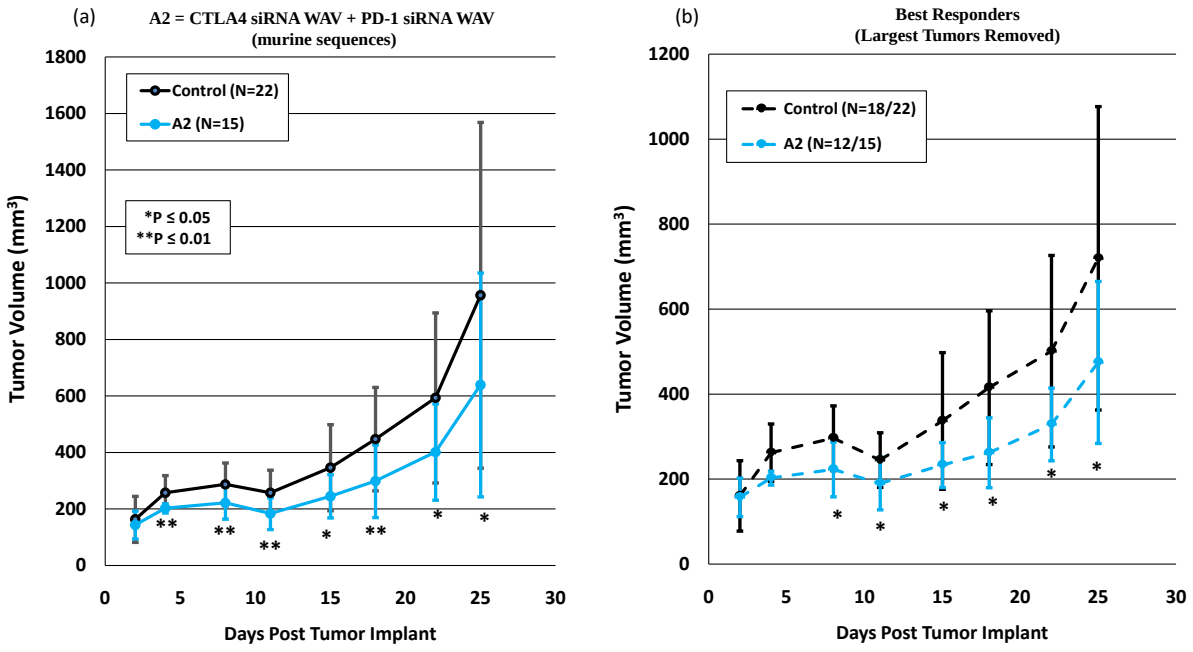

Figure 1. Average tumor volume plot for control mice (No RFE) and mice exposed to the CTLA-4/PD-1 siRNA WAV signal (A2 Signal). (a) tumor volume change over time with constant A2 signal exposure; (b) tumor volume change of best responding tumors over time with constant A2 signal exposure. Error bars are standard deviations.

At the termination of the experiments, whole blood was collected from the mice for a complete blood count (CBC). As displayed in Figure 2, no statistically

significant differences were observed in between both groups for white blood cell (WBC) counts, red blood cell (RBC) counts and platelet (PLT) counts.

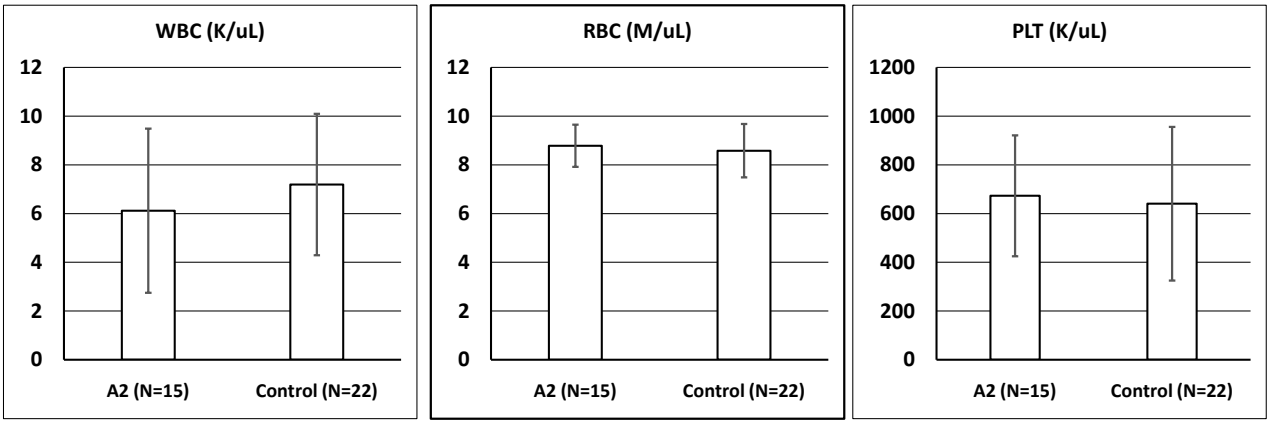

Figure 2. Cell blood counts (CBCs) at study termination for control and A2 signal exposed mice. White blood cell (WBC) values are in the thousands (K) of cells per uL. Red blood cell (RBC) values are in the millions (M) of cells per uL. Platelet counts (PLT) are in the thousands (K) of cells per uL. Error bars are standard deviation.

Additional sub-counts for polymorphonucleocytes (neutrophils), lymphocytes, monocyte and eosinophils are displayed in **Figure 3**. There was a statistically significant lower lymphocyte count in the A2 WAV exposure group when compared to the control group (P = 0.05).

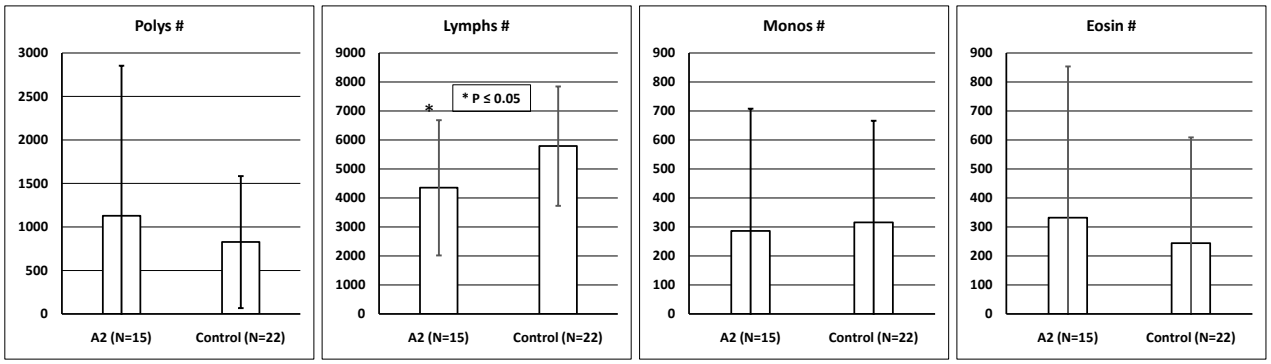

Figure 3. Cell blood counts (CBCs) at study termination for control and A2 signal exposed mice. Polymorphonucleocytes (Poly) values numbers per uL. Lymphocytes (Lymph) values are per uL. Monocytes (Monos) are per uL. Eosinophils (Eosin) are per uL. Error bars are standard deviation.

3.2. Effects of the A2 Signal on CTLA4, Pcdc-1, Ki67, CD4, CD8 and Caspase 3 Expression in Tumor Tissue

Tumor samples were snap frozen in liquid nitrogen at time of collection and prepared for delivery to a third party, independent protein analysis laboratory (Kendrick Labs). Tumors were randomly selected from the A2 WAV and control group (N = 10 per group) and the samples blinded. The staff at Kendrick Labs were unaware of the exposure that each tumor experienced.

Western blots of protein expression for CTLA4 and Pcdc-1 (PD-1) are displayed

in https://www.emulatetx.com/s/Supplement-2-PAGE-Western-Blots.pdf (pages 2-5). A total of 40 ug of protein lysate were loaded per lane for each tumor. A laser densitometry measure was applied to the entire Western blot and the band values were calibrated to the positive control band for each specific protein labeled. The band density values were derived for the bands identified between the upper and lower red lines. The individual results from the measured bands for each lane are displayed in **Figure 4(a)** (CTLA4) and **Figure 4(b)** (Pcdc-1). The average results for the protein expression values are displayed in **Figure 4(c)**.

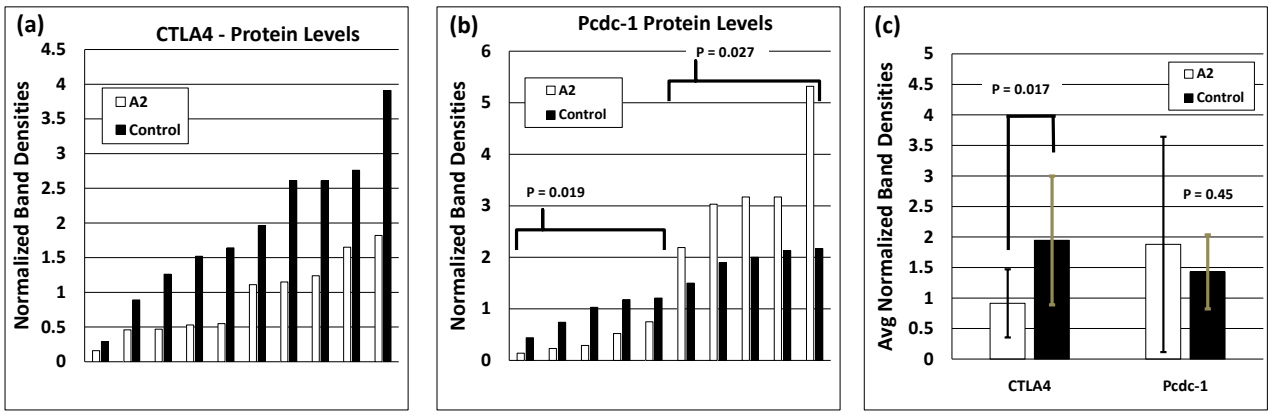

Figure 4. Plotted values of normalized band densities for CTLA4 and PD-1 Western blots. (a) CTLA4 densitometry values are normalized to the positive loading control (40 ug) for each lane; (b) Pcdc-1 densitometry values are normalized to the positive loading control (40 ug) for each lane; (c) average densitometry values for each protein blotted (a = 0.05). Error bars are standard deviation.

As displayed on **Figure 4(a)**, CTLA4 expression was reduced consistently in the A2 WAV exposure group, when compared to the Control group. In **Figure 4(b)**, Pcdc-1 expression was only reduced in half of the tumors when compared to the Control group. Comparing the average reduction in CTLA4 and Pcdc-1 protein expression demonstrated a significant reduction in the CTLA4 group (P = 0.017), but not in the Pcdc-1 group (**Figure 4(c)**).

Figure 5(a) and **Figure 5(b)** plot the individua values for Caspase 3 and Ki 67, respectively. **Figure 5(c)** plots the average band densities of Caspase 3 and Ki67. The Caspase 3 values in the A2 group were trending towards significance, but neither A2 WAV or the Control group demonstrated a statistically significant difference. Western blots of protein expression for Caspase 3 and Ki67 are displayed in https://www.emulatetx.com/s/Supplement-2-PAGE-Western-Blots.pdf (pages 6-7, 14-15).

Figure 6(a) and **Figure 6(b)** plot the individua values for CD4 and CD8 expression. **Figure 6(c)** plots the average band densities of CD4 and CD8. Both CD4 and CD8 values in the A2 group were trending towards significance, but neither A2 WAV or the Control group demonstrated a statistically significant difference. Western blots of protein expression for CD4 and CD8 are displayed in https://www.emulatetx.com/s/Supplement-2-PAGE-Western-Blots.pdf (pages 8-11).

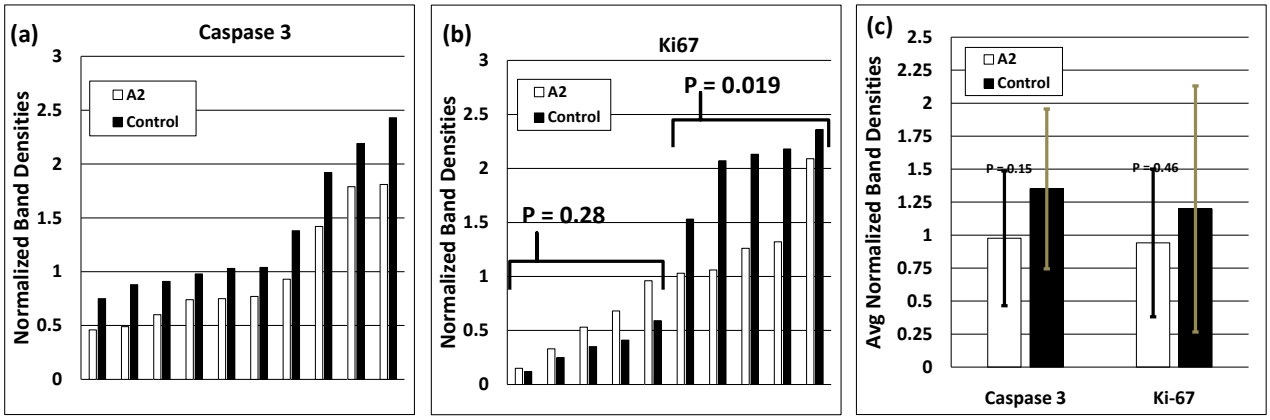

Figure 5. Plotted values of normalized band densities for Caspase 3 and Ki67 Western blots. (a) Caspase 3 densitometry values are normalized to the positive loading control (40 ug) for each lane; (b) Ki67 densitometry values are normalized to the positive loading control (40 ug) for each lane; (c) average densitometry values for each protein blotted. Error bars are standard deviation.

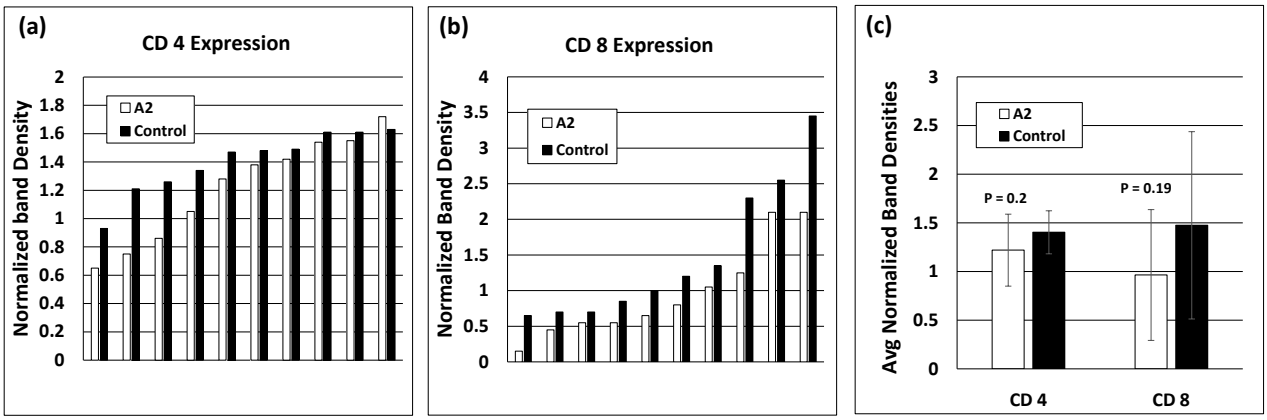

Figure 6. Plotted values of normalized band densities for CD4 and CD8 Western blots. (a) CD4 densitometry values are normalized to the positive loading control (40 ug) for each lane; (b) CD8 densitometry values are normalized to the positive loading control (40 ug) for each lane; (c) average densitometry values for each protein blotted. Error bars are standard deviation.

4. Discussion

The rationale for reducing the expression of key immune checkpoint receptors, such as CTLA-4 and PD-1 with siRNA, is based on the success of the CTLA-4 and PD-1 targeting immunoglobulin therapies [20]-[22].

We hypothesized that reducing the expression of CTLA-4 and PD-1 should result in a more effective immune response that produces a slow-down in tumor growth.

The rationale for running Western blots on tumor proteins with 10 mice per group was done to reduce cost and to produce an even sampling of the protein measures in tumors. Randomly selecting tumors from both groups allowed for unbiased detection of total protein change with balanced arms.

The exposure of the A2 signal, which is a magnetic field recording of the siRNAs targeting the murine CTLA-4 and PD-1 mRNA, resulted in the statistically significant reduction of tumor volume and reduction of CTLA-4 protein expression in

the tumors (**Figure 4(c)**). The differential contribution of the sources of the CTLA-4 protein is unknown, as both tumor and WBCs express CTLA-4. In either case, an observed decrease in CTLA-4 expression was measured in the A2 exposed group, similar to the reported reduction of EGFR mRNA expression using the same technology [10].

The PD-1 expression profile was mixed, with half of the tumors that were exposed to the A2 signal expressing a lower amount of PD-1 versus control (**Figure 4(b)**, right). The other tumors showed the opposite effect, with greater PD-1 expression than controls. The difference in the subsets of **Figure 4(b)**, left (between the controls and A2 groups) are statistically significant (data not shown), but when looked in aggregate, there is no significant difference. We are unsure as to why this occurred, as CTLA-4 expression was reduced significantly, in all tumors analyzed.

The lack of consistent PD-1 protein reduction may explain the differences observed between the absolute tumor volume changes reported between our mouse study and the result from Kesari *et al.* article [7]. The Kesari study demonstrated a stronger inhibition of tumor growth using the A2 signal than ours. Although both were statistically significant in effect, the magnitude was less in our hands. Genetic background differences may play a role, as the mouse strains used in the UCSD study [7] and the IDRI study (ours) came from two different vivariums. Unfortunately, Mukthavaram *et al.* do not report on the expression of CTLA-4, PD-1 or CBCs in their publication.

Both CTLA-4 and PD-1 are expressed in a wide variety of tumors [23] [24], but the exact mechanism by which the immune system effects tumor cell death or tumor cell growth arrest (apoptosis, necrosis or cell cycle inhibition) appears to be dependent on multiple factors.

Total tumor protein expression, specifically Caspase 3 and Ki67 (**Figure 5**), suggests that the observed reduction in tumor growth was not due primarily via apoptosis, but by a reduction in the rate of tumor cell division and potentially increased necrosis. Although the proteins levels did not reach statistical significance between the A2 and Control groups for Ki67, the protein expression differences of Caspase 3 was trending to significance. This trend suggesting a lower level of apoptosis in the A2 exposure group than the control group.

As part of a comprehensive overview of immune modulating effects of the A2 signal, we ran CBC counts on our A2 exposed and Control mice at the end of the exposure period. As displayed for the average CBC values in **Figure 2**, as an aggregate, no differences were observed in RBC, WBC and platelet values. No evidence of toxicity or alteration in baseline CBC levels was measured. Sub-analysis of WBCs (**Figure 3**) did reveal that the A2 group had a significantly reduced level of lymphocyte counts when compared to the Control group. The full values of CBCs are in https://www.emulatetx.com/s/Supplement-3-CBC-Results-Table.pdf.

In the literature, survival in patients with stage III unresectable melanoma was associated with increases in lymphocyte counts from baseline [25] after the first dose with Ipilimumab immunoglobulin infusion. In another clinical study [26],

ratios of neutrophils/lymphocytes (NLR), eosinophils/lymphocytes (ELR) and platelets/lymphocytes (PlaLR) after the second round of ipilimumab showed a lower ratio in patients from baseline values and NLR was a prognostic marker in melanoma. A measurable shift in WBC sub-populations is a consistent finding for clinically meaningful effects.

In our study, we demonstrated that exposure to the A2 signal significantly (**Figure 3**, Lymph #) lowers lymphocyte levels when compared to the Control group. When an analysis of the ratio between polymorphonucleocytes to lymphocytes (PLR), eosinophils to lymphocytes (ELR) and platelets to lymphocytes (PlaLR) was done, there was a trend towards significance (**Table 1**). Increases in the ratios between these sub-populations suggest that decreasing the expression of CTLA-4 produce changes in the immune cell numbers.

Table 1. Ratios of polymorphonucleocytes to lymphocytes (PLR), eosinophils to lymphocytes (ELR) and platelets to lymphocytes (PlaLR).

	Statistical Values				
Cell Ratios	A2 (N = 15)	Control (N = 22)	A2 SD	Control SD	P-Val
PLR	0.307	0.15	0.467	0.121	0.141
ELR	0.068	0.038	0.063	0.046	0.105
PlaLR	0.23	0.134	0.234	0.106	0.1

These alterations may be specific to our mechanism of action, a reduction in CTLA-4 expression, as compared to the infusion of immunoglobulins that target CTLA-4. The change in lymphocyte counts in our study could be indicative of an effective tumor response when CTLA-4 receptor expression is reduced. Studies in CTLA-4 conditional KO mice (tamoxifen suppressor) demonstrate a reduction of lymphocytes [27] after tamoxifen induced KO after several weeks. The report by Paterson *et al.* parallels the response we measure when CTLA-4 knock-down occurs with our A2 signal.

The reduced lymphocyte cell counts (**Figure 3**) correspond with a trend towards a lower expression of the CD4+ and CD8+ antigen cell-surface markers, as measured in Western blot analysis (**Figure 6(c)**) of the tumors analyzed. CD4+ and CD8+ T-cells are primary effector cells involved in tumor infiltration and the primary targets of the co-inhibitory and co-stimulatory axis of current immune therapies [28]. Reduction in blood lymphocyte counts coincides with the trend observed in the CD4+ and CD8+ protein expression. Although we did not directly measure the relative number of CD4+ and CD8+ T-lymphocytes between the A2 and control group, the reduction in lymphocytes could indicate an effect produced by the CTLA-4 reduction via the signal.

Previous published articles [10] demonstrated the effectiveness of the technology when emulating siRNA against mRNA and protein expression *in vitro* and *in vivo*, targeting EGFR. At the time of our A2 experimental exposures, we were limited to measuring the effects of our technology to protein expression levels in

tumors, due to budgetary and laboratory limitations. Our study design was dependent on detecting

changes in tumor volume, protein expression and immune cell alterations. Analysis of mRNA levels proved to be too costly and too technically challenging to carry out, at the time of the study. Given the evidence of an effect targeting EGFR, we felt confident in directly measuring the protein expression of these immune checkpoint receptors.

Additional support for the observed effects seen in our animal model with the human targeting of CTLA-4 and PD-1 siRNA signals is in the published results of a phase I study in recurrent glioblastoma, NAT-105 (NCT02507102) [18]. Clinical trials testing the safety and preliminary efficacy of the A2 signal in GBM patients was encouraging. The majority of patients achieved a best overall response of stable disease, and two of 15 patients achieved a partial response. The Phase I results suggest that targeting the CTLA-4 and PD-1 receptors in rGBM is a reasonable approach as part of a treatment strategy in this population.

5. Conclusion

Here we demonstrate the ability to target a reduction in the expression of at least one immune-check point inhibitor receptor (CTLA-4) in a mouse model. The exposure to the magnetic field emulations of siRNA targeting murine CTLA-4 and PD-1 resulted in significant reduction in tumor volume in the A2 exposure group as compared to the control group, replicating the results from the Kesari laboratory [7]. A significant reduction in lymphocytes was observed in the A2 group which correlated with a trend in the lowered expression of CD4 and CD8 protein in tumor samples. No safety signals, grossly or in CBCs, were observed in mice. Our results mirror the observed safety profile of the NAT-105 clinical trial. Further clinical research is supported by our pre-clinical and clinical results.

Ethics Approval and Consent to Participate

Ethical approval for the animal tumor models was approved by the IDRI IACUC. Consent to participate was not sought, as this was not a clinical trial or involved human subjects.

Availability of Data and Materials

The datasets used and/or analysed during the current study are available from the corresponding author on reasonable request.

Funding

EMulate Therapeutics, Inc. provided the funds for the experiments, as well as salaries of the authors.

Declaration

The authors declare that the experiments were done in accordance with the

ARRIVE guidelines (https://arriveguidelines.org) and all ethical approvals were done under the Infectious Disease Research Institutes (IDRI) IACUC protocols and under the supervision of the Study Director at IDRI. The authors declare that no image manipulation, other than cropping for purposes of fitting Western blot images in the figures, was done. Raw images can viewed in the https://www.emulatetx.com/s/Supplement-2-PAGE-Western-Blots.pdf materials.

Authors' Contributions

XAF was the main manuscript writer, responsible for the experimental design and data interpreter. BMB invented the MIDS, recorded the A1A & A2 signal, contributed to the manuscript and provided editorial input. GV designed the small inhibitor RNAs that were recorded, wrote sections of the manuscript and the supplements and provided editorial input on the manuscript.

Acknowledgements

We would like to thank Dr. Winston Wicomb (Study Director) and his staff at IDRI for the work that was done on the murine tumor models.

Conflicts of Interest

The authors declare no conflicts of interest regarding the publication of this paper. All three authors were paid employees and/or contractors when the work for this manuscript was done. All three authors are also stockholders in EMulate Therapeutics, inc.

References

[1] Thomas, Y., Schiff, M., Belkadi, L., Jurgens, P., Kahhak, L. and Benveniste, J. (2000) Activation of Human Neutrophils by Electronically Transmitted Phorbol-Myristate Acetate. *Medical Hypotheses*, **54**, 33-39. https://doi.org/10.1054/mehy.1999.0891

[2] Smith, J.A. and Weidemann, M.J. (1993) Further Characterization of the Neutrophil Oxidative Burst by Flow Cytometry. *Journal of Immunological Methods*, **162**, 261-268. https://doi.org/10.1016/0022-1759(93)90391-j

[3] Roy, D.K., Balanarayan, P. and Gadre, S.R. (2009) Signatures of Molecular Recognition from the Topography of Electrostatic Potential. *Journal of Chemical Sciences*, **121**, 815-821. https://doi.org/10.1007/s12039-009-0097-5

[4] Kloes, G., Bennett, T.J.D., Chapet-Batlle, A., Behjatian, A., Turberfield, A.J. and Krishnan, M. (2022) Far-field Electrostatic Signatures of Macromolecular 3D Conformation. *Nano Letters*, **22**, 7834-7840. https://doi.org/10.1021/acs.nanolett.2c02485

[5] Carvalho, C.S., Vlachakis, D., Tsiliki, G., Megalooikonomou, V. and Kossida, S. (2013) Protein Signatures Using Electrostatic Molecular Surfaces in Harmonic Space. *PeerJ*, **1**, e185. https://doi.org/10.7717/peerj.185

[6] Butters, J.T., Figueroa, X.A. and Butters, B.M. (2014) Non-Thermal Radio Frequency Stimulation of Tubulin Polymerization *in Vitro*: A Potential Therapy for Cancer Treatment. *Open Journal of Biophysics*, **4**, 147-168. https://doi.org/10.4236/ojbiphy.2014.44015

[7] Mukthavaram, R., Jiang, P., Pastorino, S., Nomura, N., Lin, F. and Kesari, S. (2024) Evaluation of the Emulate Therapeutics Voyager's Ultra-Low Radiofrequency Energy in Murine Model of Glioblastoma. *Bioelectronic Medicine*, **10**, Article No. 10. https://doi.org/10.1186/s42234-024-00143-8

[8] Qiu, B., Sun, X., Zhang, D., Wang, Y., Tao, J. and Ou, S. (2012) TRAIL and Paclitaxel Synergize to Kill U87 Cells and U87-Derived Stem-Like Cells *in Vitro*. *International Journal of Molecular Sciences*, **13**, 9142-9156. https://doi.org/10.3390/ijms13079142

[9] Barkhoudarian, G., Badruddoja, M., Blondin, N., Chowdhary, S., Cobbs, C., Duic, J.P., *et al.* (2023) An Expanded Safety/feasibility Study of the Emulate Therapeutics Voyager™ System in Patients with Recurrent Glioblastoma. *CNS Oncology*, **12**, CNS102. https://doi.org/10.2217/cns-2022-0016

[10] Ulasov, I.V., Foster, H., Butters, M., Yoon, J., Ozawa, T., Nicolaides, T., *et al.* (2017) Precision Knockdown of EGFR Gene Expression Using Radio Frequency Electromagnetic Energy. *Journal of Neuro-Oncology*, **133**, 257-264. https://doi.org/10.1007/s11060-017-2440-x

[11] Rekulapelli, A., Flausino, L., Iyer, G. and Balkrishnan, R. (2022) Effectiveness of Immunological Agents in Non-Small Cell Lung Cancer. *Cancer Reports*, **6**, e1739. https://doi.org/10.1002/cnr2.1739

[12] Reck, M., Ciuleanu, T., Cobo, M., Schenker, M., Zurawski, B., Menezes, J., *et al.* (2023) First-line Nivolumab Plus Ipilimumab with Two Cycles of Chemotherapy versus Chemotherapy Alone (Four Cycles) in Metastatic Non-Small Cell Lung Cancer: Checkmate 9LA 2-Year Patient-Reported Outcomes. *European Journal of Cancer*, **183**, 174-187. https://doi.org/10.1016/j.ejca.2023.01.015

[13] Muto, I., Koga, H., Doi, R., Katayama, E., Nakama, K. and Nakama, T. (2022) Efficacy of Nivolumab and Ipilimumab Combined Therapy as a First-Line Therapy for Patients with Advanced Melanoma and the Urgent Need for an Effective Second-Line Therapy for Patients with Wild-Type BRAF in Japan: A Single Center Retrospective Study. *The Kurume Medical Journal*, **69**, 75-80. https://doi.org/10.2739/kurumemedj.ms6912008

[14] VanderWalde, A., Bellasea, S.L., Kendra, K.L., Khushalani, N.I., Campbell, K.M., Scumpia, P.O., *et al.* (2023) Ipilimumab with or without Nivolumab in PD-1 or PD-L1 Blockade Refractory Metastatic Melanoma: A Randomized Phase 2 Trial. *Nature Medicine*, **29**, 2278-2285. https://doi.org/10.1038/s41591-023-02498-y

[15] Li, H., Li, H., Tang, L., Niu, H., He, L. and Luo, Q. (2023) Associations between Immune-Related Venous Thromboembolism and Efficacy of Immune Checkpoint Inhibitors: A Systematic Review and Meta-Analysis. *Clinical and Applied Thrombosis/Hemostasis*, **29**, 10760296231206799. https://doi.org/10.1177/10760296231206799

[16] Zhu, Y., Liu, K., Zhu, H., Cao, H. and Zhou, Y. (2023) Comparative Efficacy and Safety of Novel Immuno-Chemotherapy for Extensive-Stage Small-Cell Lung Cancer: A Network Meta-Analysis of Randomized Controlled Trial. *Therapeutic Advances in Medical Oncology*, **15**, 17588359231206147. https://doi.org/10.1177/17588359231206147

[17] Awan, S., Bharucha, P., Steventon, L., Simpson, H., AHMAD, T., Benafif, S., *et al.* (2023) Out-of-hours Admissions in Patients Treated with Immune Checkpoint Inhibitors and Their Primary Management with Steroids. *Journal of Oncology Pharmacy Practice*. https://doi.org/10.1177/10781552231207271

[18] Murphy, M., Dowling, A., Thien, C., Priest, E., Morgan Murray, D. and Kesari, S. (2019) A Feasibility Study of the Nativis Voyager® Device in Patients with Recurrent

Glioblastoma in Australia. *CNS Oncology*, **8**, CNS31.
https://doi.org/10.2217/cns-2018-0017

[19] Cobbs, C., McClay, E., Duic, J.P., Nabors, L.B., Morgan Murray, D. and Kesari, S. (2018) An Early Feasibility Study of the Nativis Voyager® Device in Patients with Recurrent Glioblastoma: First Cohort in US. *CNS Oncology*, **8**, CNS30.
https://doi.org/10.2217/cns-2018-0013

[20] Camacho, L.H. (2015) CTLA-4 Blockade with Ipilimumab: Biology, Safety, Efficacy, and Future Considerations. *Cancer Medicine*, **4**, 661-672.
https://doi.org/10.1002/cam4.371

[21] Sun, Q., Hong, Z., Zhang, C., Wang, L., Han, Z. and Ma, D. (2023) Immune Checkpoint Therapy for Solid Tumours: Clinical Dilemmas and Future Trends. *Signal Transduction and Targeted Therapy*, **8**, Article No. 320.
https://doi.org/10.1038/s41392-023-01522-4

[22] Wang, F., Xia, T., Li, Z., Gao, X. and Fang, X. (2023) Current Status of Clinical Trial Research and Application of Immune Checkpoint Inhibitors for Non-Small Cell Lung Cancer. *Frontiers in Oncology*, **13**, Article 1213297.
https://doi.org/10.3389/fonc.2023.1213297

[23] Kumar, P., Bhattacharya, P. and Prabhakar, B.S. (2018) A Comprehensive Review on the Role of Co-Signaling Receptors and Treg Homeostasis in Autoimmunity and Tumor Immunity. *Journal of Autoimmunity*, **95**, 77-99.
https://doi.org/10.1016/j.jaut.2018.08.007

[24] Kim, M.J. and Ha, S. (2021) Differential Role of PD-1 Expressed by Various Immune and Tumor Cells in the Tumor Immune Microenvironment: Expression, Function, Therapeutic Efficacy, and Resistance to Cancer Immunotherapy. *Frontiers in Cell and Developmental Biology*, **9**, Article 767466.
https://doi.org/10.3389/fcell.2021.767466

[25] Martens, A., Wistuba-Hamprecht, K., Yuan, J., Postow, M.A., Wong, P., Capone, M., *et al.* (2016) Increases in Absolute Lymphocytes and Circulating $CD4^+$ and $CD8^+$ T Cells Are Associated with Positive Clinical Outcome of Melanoma Patients Treated with Ipilimumab. *Clinical Cancer Research*, **22**, 4848-4858.
https://doi.org/10.1158/1078-0432.ccr-16-0249

[26] Khoja, L., Atenafu, E.G., Templeton, A., Qye, Y., Chappell, M.A., Saibil, S., *et al.* (2016) The Full Blood Count as a Biomarker of Outcome and Toxicity in Ipilimumab-treated Cutaneous Metastatic Melanoma. *Cancer Medicine*, **5**, 2792-2799.
https://doi.org/10.1002/cam4.878

[27] Paterson, A.M., Lovitch, S.B., Sage, P.T., Juneja, V.R., Lee, Y., Trombley, J.D., *et al.* (2015) Deletion of CTLA-4 on Regulatory T Cells during Adulthood Leads to Resistance to Autoimmunity. *Journal of Experimental Medicine*, **212**, 1603-1621.
https://doi.org/10.1084/jem.20141030

[28] Kumar, S., Singh, S.K., Rana, B. and Rana, A. (2021) Tumor-Infiltrating $CD8^+$ T Cell Antitumor Efficacy and Exhaustion: Molecular Insights. *Drug Discovery Today*, **26**, 951-967. https://doi.org/10.1016/j.drudis.2021.01.002